 ©2011 Kvantovaya Elektronika and Turpion Ltd

PACS numbers: 42.55.Rz; 42.55.Xi; 42.60.Da; 42.15.Fr
DOI: 10.1070/QE2011v041n06ABEH014608

Operation conditions for a picosecond laser with an aberration thermal lens under longitudinal pulsed diode pumping*

V.B. Morozov, A.N. Olenin, V.G. Tunkin, D.V. Yakovlev

***Abstract*. The dependence of the repetition frequency range that provides stable operation of a picosecond laser with longitudinal pulsed diode pumping on the parameters of the laser cavity and the thermal lens induced in the active element is analysed. The results of calculating the radius of the lower cavity mode as a function of pump beam average power and diameter are reported. Based on the measurements by the probe-beam method, the adequacy of the presented model of aberration thermal lens is demonstrated for the cases of uniformly doped Nd : YAG and composite YAG/Nd : YAG active elements upon tuning the pump pulse repetition frequency within the range of 0 – 1 kHz. The ways for implementing stable generation of millijoule pulses in a specified repetition frequency range are discussed.**

Keywords: *picosecond laser, diode pumping, thermal lens.*

1. Introduction

Picosecond lasers with a high peak power (about 1 mJ or more per pulse), with repetition frequencies from several Hz to several kHz, are widely used in many research and applied problems, such as nonlinear spectroscopy [1, 2], spectrophotometry of semiconductors [3], nanobiophotonics [4], high-precision treatment of materials [5], laser surgery [6], contactless cleaning of the surface of objects of art [7], laser location [8], etc. In some practical cases picosecond lasers have advantages over femtosecond ones due to the use of simpler amplification schemes, nonlinear transformation, and transmission through optical elements and atmosphere.

The use of diode pumping, both continuous [9] and pulsed (pulsed-periodic) [10], makes it possible to design compact laser systems characterised by high stability and reliability. When repetition frequencies up to several kHz (the limiting value is determined by the lifetime of the upper laser level) are used, pulsed pumping may have certain advantages for Nd-doped active media. In this case, the energy efficiency of the conversion of the pump energy into output radiation reaches a maximum, with a minimum corresponding heat release. As a result, one can work without a water cooling circuit even when laser diode bars with a high peak power are used.

The thermal effect on the laser cavity elements, which is caused by heating diode bars, can be excluded using bars with a fibre output. This is especially important for lasing with a high average power. Longitudinal pump geometry is also convenient due to the possibility of effective amplification of the radiation generated at the lower Gaussian cavity mode, without taking any measures for spatial mode selection. At the same time, the highly inhomogeneous radial distribution of the pump intensity in the laser active element (AE) leads to the formation of an aberration thermal lens [11], in contrast to the cases of fairly uniform lamp [12] or transverse diode pumping [13], where the thermal lens remains almost spherical in a wide range of pump powers and can be compensated for by conventional optical elements. In the case of longitudinal pumping the thermal lens consists of an easily compensated parabolic part and an aberration part, which is much more difficult to compensate for [14]. The character of the aberration component is determined by the spatial distribution of the pump intensity, parameters of the AE, and the heat sink conditions.

When the average pump power reaches some value, aberrations lead to higher losses and disturb mode locking. As a result, stable generation of millijoule pulses becomes impossible even at repetition frequencies of several hundreds of Hz. One cannot increase the peak pump power to compensate for aberration losses, which grow faster than the amplification. This is a kind of payment for the convenience of using the longitudinal diode pump geometry. In this paper, we report the results of the experimental and theoretical analysis of the thermal lens in the AE of a picosecond laser with a pulsed longitudinal diode pumping in order to determine the conditions of its effective and stable operation at repetition frequencies up to ~ 1 kHz.

2. Simulation of the laser cavity

The optical scheme of a picosecond laser is shown in Fig. 1. Two coupled zig-zag cavities [15] have a common AE with a length $l_{ac} = 11$ mm and a diameter $d_{ac} = 5$ mm, with a

*Reported at the conference 'Laser Optics', Russia, St. Petersburg, June 2010

V.B. Morozov, A.N. Olenin, V.G. Tunkin Department of Physics, M.V. Lomonosov Moscow State University, Vorob'evy Gory, 119991 Moscow, Russia; e-mail: morozov@phys.msu.ru, andrei_olenin@mail.ru, vladimirtunkin@mail.ru;
D.V. Yakovlev International Laser Center, M.V. Lomonosov Moscow State University, Vorob'evy Gory, 119991 Moscow, Russia; e-mail: dmyak@mail.ru

Received 24 February 2011
Kvantovaya Elektronika **41** (6) 508 – 514 (2011)
Translated by Yu.P. Sin'kov

Nd concentration of 1.1 %, pumped by a pulsed diode bar with a fibre output (maximum peak power $P_{max} = 70$ W, wavelength 808 nm). Pump pulses with a width $\tau_p = 200$ μs and repetition frequencies f_p in the range of 0–1000 Hz from the output of a fibre 0.6 mm in diameter are focused into the AE through the cavity terminal mirror M1. In the experiments the maximum peak pump power is limited at the level of 55 W. The thermal contact of the lateral surface of AE with the aluminium air-cooled heat sink is provided by an indium layer. Since the thermal conductivities of indium and aluminium exceed that of YAG by factors of about 6 and 10, respectively, [16], and the end surfaces of the AE are only convection-cooled, we assume that its lateral surface has a fixed temperature and neglect the heat flux through the end faces.

The first cavity is formed by a convex mirror M1 and a semiconductor saturating mirror SM with a modulation depth of 8 % and recovery time of 10 ps. A concave mirror M2 is placed near the centre of the cavity. This highly reflecting cavity is aimed at forming a picosecond pulse with an energy of ~ 1 μJ under signals of negative feedback and active mode locking (AML), which are applied to a two-crystal electro-optical modulator EOM1 from an RTP crystal [15] at the end of each pump pulse. Passive mode locking by the semiconductor mirror SM allows one to reduce the pulse formation time to 5–10 μs and thus shorten the pulse. The picosecond pulse energy is amplified to 1–1.5 mJ by a regenerative amplifier, the cavity of which is formed by the mirrors M1 and M3. The cavities are switched by applying a half-wave voltage pulse to an electro-optical modulator EOM2. The radiation is extracted from the amplifier cavity by applying a quarter-wave voltage pulse across the modulator EOM3.

The distance L_1 between the mirror M1 and the AE is chosen to be 1 cm to exclude the formation of a standing wave near the cavity end mirror [17] when generating pulses with a width of about 25 ps. The optical length of the first cavity, $L_{res} = 145$ cm, corresponds to the quarter period of the AML harmonic signal, and the distance L_2 between the AE and mirror M2 is 69 cm. In this configuration the distance between EOM2 and M1 is sufficiently large to ensure the modulator actuation over the time during which the optical pulse passes this distance in the forward and backward directions. The spherical mirrors M1 and M2 provide cavity stability. The radius of curvature R_1 of the convex mirror M1 is such as to compensate for the parabolic component of the thermal lens in the active crystal. The average diameter of the cavity mode is mainly determined by the radius of curvature R_2 of the concave mirror M2.

The equivalent optical scheme of both cavities, which is used to calculate the mode radius, is presented in Fig. 2a. Here, the concave mirror M2 is replaced by a lens L with a focal distance $F = R_2/2$. Since the mutual arrangement of the cavity optical elements is fixed, the configuration of the cavity mode is completely determined by the parameters R_1 and F and by the thermal lens induced in the AE. The latter is considered to be thin because the length of the heated region corresponds to the pump absorption length $l_a \sim 3$ mm, which is small in comparison with other distances in this scheme.

The behaviour of the cavity mode with a change in the pump pulse repetition frequency f_p is analysed based on the following simple model of a thermally induced lens. The distribution of the pump intensity in the AE within a cylindrical region with a length l_a and a radius r_p (Fig. 2b) is assumed to be uniform. The pump radiation

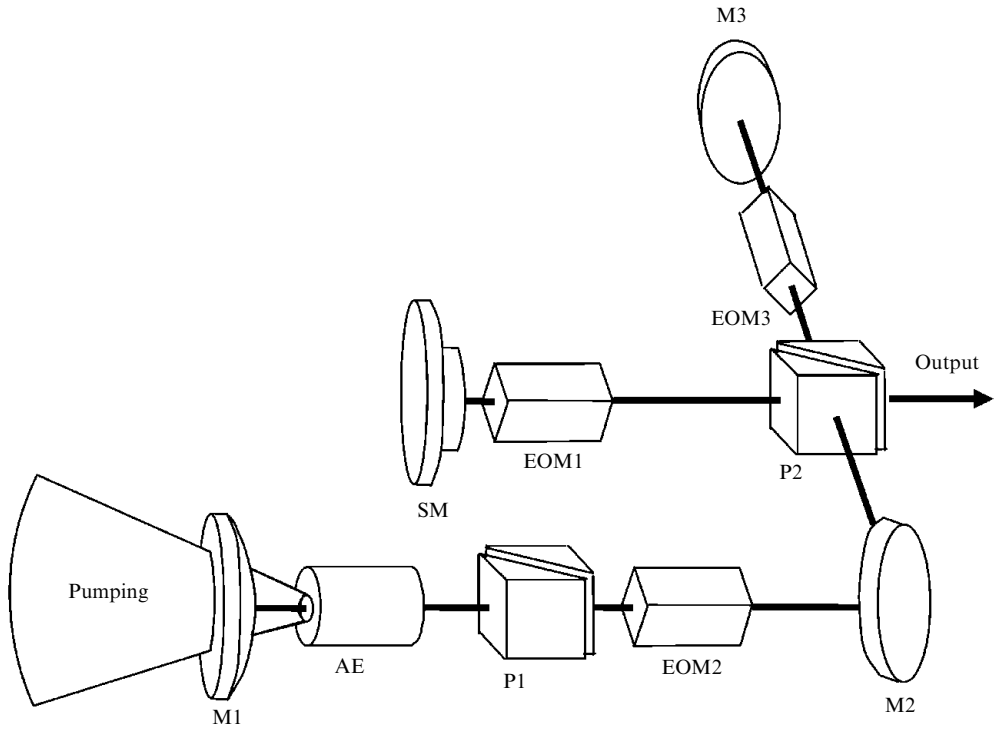

Figure 1. Simplified optical scheme of a picosecond laser: (M1) convex mirror, (AE) active element, (EOM1, EOM2, EOM3) electro-optical modulators, (M2) concave mirror, (P1, P2) polarisers, (SM) saturating semiconductor mirror, and (M3) flat mirror.

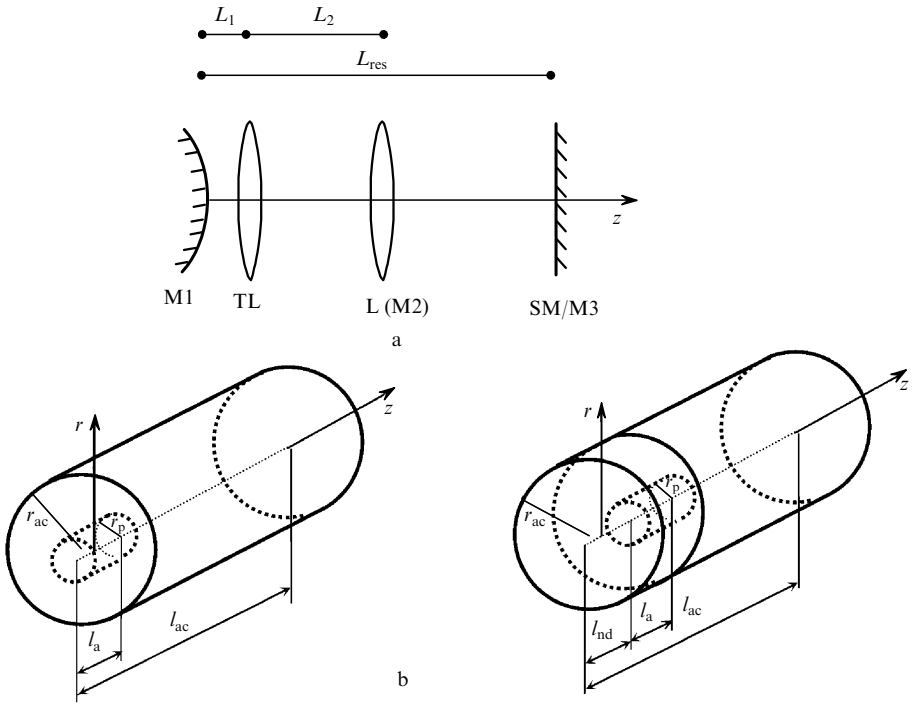

Figure 2. Equivalent schemes of (a) the cavity and (b) the AE with an isolated pumped region for Nd : YAG and YAG/Nd : YAG (on the left and right, respectively): TL is the thermal lens; r_{ac} and r_p are, respectively, the radii of the AE and the pumped region; l_{ac} and l_{nd} are the lengths of the active crystal and the undoped region, respectively; and l_a is the length of the pumped region.

is a sequence of rectangular pulses of width τ_p and repetition period $1/f_p$. A simple estimation based on the value of the AE specific heat [18] shows that each pump pulse increases the temperature in the AE absorbing region by several tenths of a kelvin. Thus, lasing is not accompanied by a significant change in the temperature distribution in the AE, and the pulsed thermal effect of pumping can be replaced by a stationary effect with the same average power. Furthermore, we will consider two mechanisms of thermal lens formation: (i) based on the temperature dependence of the refractive index and (ii) strain due to the thermal expansion of the laser crystal surface through which pumping is performed [19]. The focusing properties of the thermal lens are determined by the radial dependence of the additional (heating-induced) optical path length ΔL^T of radiation in the AE, which can be expressed in terms of the integral of the temperature distribution [14]:

$$\Delta L^T_{2D}(r) = \left[\frac{dn}{dT} + (1+\nu)(n_0-1)\alpha_T\right]\int_0^{l_{ac}} T(r,z)dz, \qquad (1)$$

where the following AE parameters are used: dn/dT is the thermooptical coefficient; α_T is the thermal expansion coefficient; ν is the Poisson coefficient; and n_0 is the refractive index.

The temperature distribution $T(r,z)$ can be found from the heat-conduction equation. In the case of cylindrical symmetry we have a two-dimensional problem in the coordinates (r,z) (Fig. 2b) [20]:

$$\frac{d^2T(r,z)}{dr^2} + \frac{1}{r}\frac{dT(r,z)}{dr} + \frac{d^2T(r,z)}{dz^2} + \frac{Q(r,z)}{k_T} = 0. \qquad (2)$$

Here, $Q(r,z)$ is the power density of heat sources and k_T is the heat conductivity. The numerical solution of Eqn (2) shows that, if heat is removed only through the lateral AE surface, the temperature distribution along the z axis is almost rectangular (Fig. 3a). This fact indicates that radial heat fluxes dominate in the AE. Thus, it is reasonable to solve the one-dimensional heat-conduction problem:

$$\frac{d^2T(r)}{dr^2} + \frac{1}{r}\frac{dT(r)}{dr} + \frac{Q(r)}{k_T} = 0. \qquad (3)$$

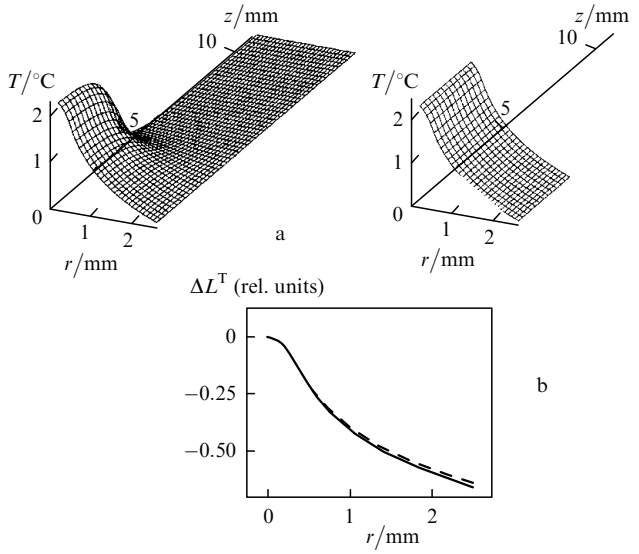

Figure 3. (a) Calculated temperature distributions in a cylindrical AE at the same heating power density and heat removal through only the lateral surface: two-dimensional dependence in the coordinates r and z (on the left) and one-dimensional radial dependence (on the right). (b) Dependences of the optical path length in the AE on the radial coordinate in the presence of a thermal lens, calculated for the one-dimensional (dashed line) and two-dimensional (solid line) cases.

Having substituted the solution of Eqn (3) into expression (1), we obtain

$$\Delta L_{1D}^{T} = \left[\frac{dn}{dT} + (1+\nu)(n_0 - 1)\alpha_T\right] \times \frac{Q_0 r_p^2 l_a}{4k_T} \begin{cases} -2\ln\dfrac{r_p}{r_{ac}} + 1 - \dfrac{r^2}{r_p^2}, & r \leqslant r_p, \\ -2\ln\dfrac{r}{r_{ac}}, & r_p < r \leqslant r_{ac}, \end{cases} \quad (4)$$

where Q_0 is the power density of a uniform equivalent heat source in the pumped region. Indeed, as can be seen in Fig. 3b, the results of calculating ΔL^T in two- and one-dimensional cases are very similar. To obtain a certain focal distance of the thermal lens, we will retain only the term quadratic in r in expression (4). This simplification allows us to write the focal distance of the thermal lens, F_{tl}, in the form [19]

$$F_{tl} = \frac{2\pi k_T r_p^2}{\gamma P_p[(dn/dT) + (1+\nu)(n_0 - 1)\alpha_T]}, \quad (5)$$

where $\gamma = 1 - \lambda_p/\lambda_{las}$ is the part of pump energy converted into heat, λ_p is the pump wavelength, and λ_{las} is the lasing wavelength. The average pump power can be written as

$$P_p = \frac{P_{max}\tau_p f_p (I - I_0)}{I_{max} - I_0},$$

where I_{max}, I_0, and I are, respectively, the maximum, threshold, and working currents of the diode bar.

The radius of the lower Gaussian mode was calculated using the formalism of ABCD matrices [21], taking into account the aforementioned parameters of the cavity and the focal distance of the thermal lens, which is determined by formula (5). In this study we disregard the effect of the amplification in the AE and the absorption in the semiconductor mirror (processes that depend on the radiation intensity) on the cavity mode formation. The features of the optical scheme under consideration and the total cavity length are mainly determined by the requirements imposed by the regimes of electro-optical negative feedback and active mode locking in the case of picosecond pulses. Obviously, the proposed approach to determination of the thermal lens parameters and the conditions for lasing stability can also be applied to other types of lasers with longitudinal pulsed diode pumping.

3. Diagrams of cavity stability

Stable laser operation at high repetition frequencies is determined to a great extent by the thermal regime of the key elements, such as the pump module and the electro-optical modulators. In this case, the mode locking regime appears to be extremely vulnerable. In this section we will discuss the conditions for lasing stability, which are determined by the necessity of matching the cavity mode with the apertures of its optical elements with a change in the thermal lens parameters, which is determined by the choice of the repetition frequency and the diameter of the pumped region. Stable lasing can be implemented in only limited ranges of variation in the parameters.

The longitudinal profile of the cavity mode was calculated for different sets of R_1 and F, taking into account the presence of the thermal lens. The range of cavity stability is determined by the values of the focal distance of the thermal lens at which the mode does not emerge beyond the apertures of the optical elements. Examples of stability diagrams are shown in Fig. 4. Larger values of r_p correspond to wider ranges of possible tuning the pump pulse repetition frequency (Fig. 4b). At the same time, as soon as r_p exceeds the mode radius, the pump efficiency drops [22]. Small r_p values provide a good overlap of the pump beam with the cavity mode, but all diagrams are characterised by a narrow tuning range (Fig. 4a). An analysis of the behaviour of the curves corresponding to a fixed F value shows that a decrease in R_1 (increase in the curvature of the mirror M1) shifts the diagram as a whole toward higher repetition frequencies, at which the thermal lens is compensated for. An increase in the focal distance F at a fixed R_1 also leads to an increase in the mode radius and shift of the diagram to

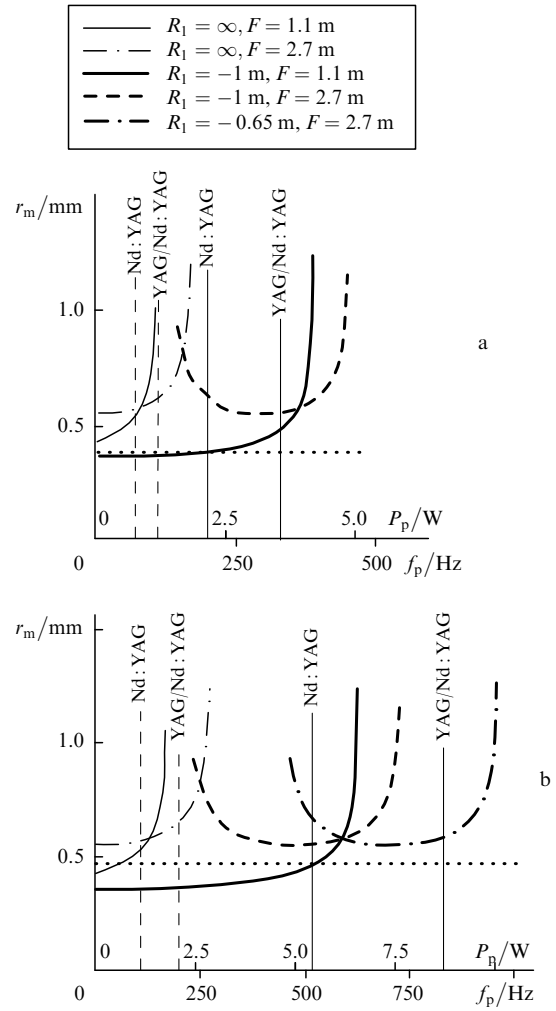

Figure 4. Dependences of the mode radius r_m in the AE on the average pump power and the pump pulse repetition frequency for different cavity configurations and radii of the pumped region of (a) 370 and (b) 470 μm. The regions of finite sizes of the mode correspond to the ranges of stable lasing. The vertical lines separate the region of insignificant (top) and significant (bottom) effect of aberrations on the laser operation for $F = 1.1$ m (solid line) and 2.7 m (dashed line). The dotted lines indicate the radius of the pumped region.

higher repetition frequencies. Thus, having chosen the appropriate R_1 and F values, one can provide the desired position of the best stability region. However, one must take into account that a significant increase in the repetition frequency, with an invariable diameter of the pumped region, is accompanied by the enhanced effect of the aberration part of the thermal lens, which deteriorates the conditions of lasing, up to its degradation.

4. Measurement of thermal-lens aberrations

The setup for measuring the phase distortions introduced by the thermal lens is schematically shown in Fig. 5. An AE, similar to that used in the working laser, was placed in a similar aluminium heat sink with an indium layer and pumped by the same diode bar. The output radiation of a working laser at a relatively low repetition frequency was used as a probe beam (the quality factor $M^2 = 1.2$), which was transmitted through the AE pumped in the longitudinal geometry. The necessary probe-beam radius was chosen by applying an additional long-focal-length lens (is not shown). This lens was displaced along the beam axis to provide maximum filling of the AE with radiation, without any significant diffraction from its aperture. A measuring lens with a focal distance $F_L = 50$ mm was used to transform the phase distortions of the probe beam, introduced by the thermal lens, into the beam intensity distribution. The probe beam intensity profile near the focal plane of the measuring lens was recorded by a CCD camera. Since the pulsed diode bars of the pump systems of the AE under study and the probe laser were not synchronised, we rejected the images corresponding to the cases where the probe picosecond pulses coincided with the pump pulses heating the AE. The radius of the pumped region in these experiments was 370 μm; it was found from the condition of minimum lasing threshold at low repetition frequencies. To measure the transverse size of the pumped region, its image was recorded against the background of the AE aperture with a radius $r_{ac} = 2.5$ mm using a long-focal-length objective and a CCD camera.

The aberrations were measured using a uniformly doped Nd : YAG (Fig. 2b, left) and composite YAG/Nd : YAG (Fig. 2b, right) AEs. The second element has an undoped region of a length $l_{nd} = 3$ mm, through which pumping is performed. Hence, the mechanism of thermal lens formation due to the input face bending as a result of thermal expansion can be excluded. Examples of measured profiles of probe beam intensity are shown in Fig. 5. At $r_p = 370$ μm the intensity profiles remain almost Gaussian up to the repetition frequencies of 210 Hz for Nd : YAG and 350 Hz for YAG/Nd : YAG. At higher repetition frequencies the intensity profiles change significantly, and lasing is impossible in any cavity configuration. Aberrations can be reduced by increasing the pumped region radius; however, this can be done only at the expense of reduced pump efficiency.

5. Modelling aberrations

The validity of the simplest aberration model for describing experimental results was checked by comparing the measured intensity profiles and the profiles obtained by modelling the probe beam propagation. The initial radius and wavefront curvature of the probe beam were determined on the basis of the formalism of ABCD matrices with the used configuration of laser cavity. The beam propagation in free space is modelled by applying the diffraction integral [23]

$$E(P) = \frac{\mathrm{i}}{\lambda}\iint_{\Sigma} E_0(M)\frac{\mathrm{e}^{-\mathrm{i}k\rho}}{\rho}(1+\cos\theta)\mathrm{d}\sigma, \qquad (6)$$

where $E(P)$ is the electric field of laser radiation at a certain point of space P; λ is the wavelength; k is the wave vector; $E_0(M)$ is the known electric field of radiation at a point M

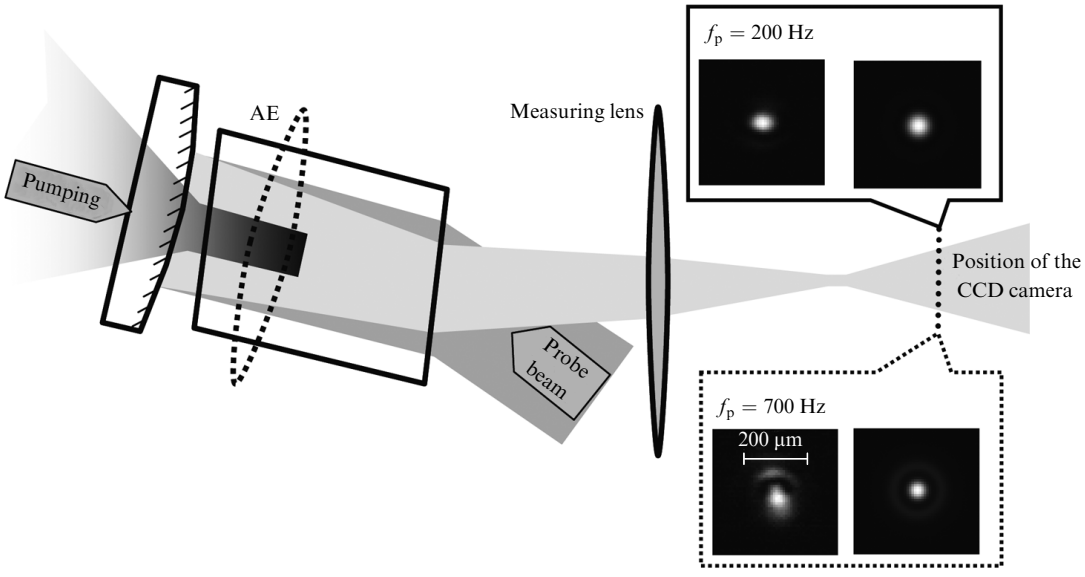

Figure 5. Schematic of the setup for measuring the thermal-lens aberrations with a change in the pump pulse repetition frequency and examples of the measured (on the left) and calculated (on the right) intensity profiles of the probe beam near the focal plane of the measuring lens for the cases of weak (top) and strong (bottom) thermal-lens aberrations in the Nd : YAG .

of some surface Σ; ρ is the length of the segment connecting the points P and M; θ is the angle between this segment and the normal to Σ; and $d\sigma$ is a surface element.

The lenses in the probe beam path and the thermal lens in the AE are considered as thin phase screens with a complex transfer function [23] $T(r)$ and the focal distance f:

$$T(r) = \exp\left(ik\frac{r^2}{2f}\right). \tag{7}$$

The AE transfer function has the form

$$T_{ac}(r) = \exp[i2k\Delta L_{1D}^{T}(r)]. \tag{8}$$

The modelling for a composite AE differs by formal equating the coefficient α_T to zero in the expression for $\Delta L_{1D}^{T}(r)$ (4).

The calculation results, which are in agreement with the corresponding experimental data, are shown in Fig. 5. It can clearly be seen that the presented model of aberration thermal lens adequately describes the probe beam distortion; at the same time, the model does not use any fitting parameters. To estimate the energy loss caused by the nonparabolic component of the thermal lens, we will consider aberrations as a wavefront perturbation for the lower Gaussian mode of the laser cavity. This perturbation increases the divergence of the initial Gaussian beam and, therefore, causes additional diffraction losses of radiation in a current pass through the cavity. The fraction of the aberration energy loss at a pass through the cavity can be estimated as follows [24]:

$$\gamma_a = \left| \frac{\int_0^{r_{ac}/\sqrt{2}r_{las}} \exp[i2\varphi(\sqrt{2}\rho r_{las}) - \rho^2]\rho d\rho}{\int_0^{r_{ac}/\sqrt{2}r_{las}} \exp(-\rho^2)\rho d\rho} \right|, \tag{9}$$

where r_{las} is the radius of the Gaussian laser mode in AE and $\varphi(\sqrt{2}\rho r_{las})$ is the phase delay induced by the thermal lens (with the quadratic component subtracted). Assuming that the acceptable level of aberration energy loss upon beam transmission through the AE, at which lasing remains stable, is 20 % [25], and using expression (4) to calculate the phase delay,

$$\varphi(r) = k\left[\frac{dn}{dT} + (1+\nu)(n_0-1)\alpha_T\right] \times \frac{Q_0 r_p^2 l_a}{4k_T} \begin{cases} 0, & r \leqslant r_p, \\ -2\ln\dfrac{r}{r_p} - 1 + \dfrac{r^2}{r_p^2}, & r_p < r \leqslant r_{ac}, \end{cases} \tag{10}$$

one can obtain [using (9)] the range of r_p/r_{las} ratios at which the aberration loss does not exceed a specified value at different pump pulse repetition frequencies (Fig. 6). As was noted above, the mode radius is determined mainly by the choice of the radius of curvature of the concave mirror M2. Based on the values of r_p and the minimum radius of the laser mode, which is determined by the choice of M2 (Fig. 4), and using the diagrams in Fig. 6, one can find the maximum values of the pump pulse repetition frequencies at which the aberration energy loss is still below 20 %. The vertical lines in Fig. 4 indicate such frequencies for different combinations of M2 and AE.

Based on the modelling results (Fig. 6), one can determine the repetition frequency range in which the losses due to the thermal lens aberrations are insignificant at a certain ratio between the pumped region radius and the laser-mode radius in the AE. For example, the aberration losses are low, and lasing may occur at a change in f_p up to 1 kHz at the r_p/r_{las} ratio equal to 1.5 for Nd : YAG and 1.37 for YAG/Nd : YAG.

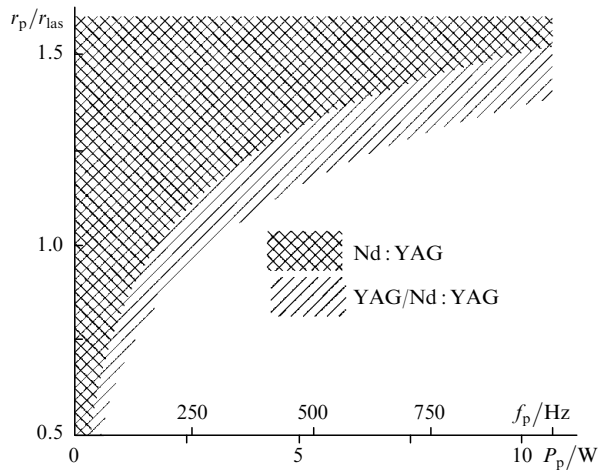

Figure 6. Diagram of the energy loss caused by thermal-lens aberrations after the pass of a Gaussian beam through the AE, depending on the pump pulse repetition frequency and the ratio of the radius of the pumped region to the beam radius for the Nd : YAG and YAG/Nd : YAG laser elements. The hatched region corresponds to the loss level below 20 %.

The conditions for stable operation of the laser used in our experiments were fulfilled up to frequencies of 400 – 450 Hz at a pumped region radius of 370 μm. A further increase in the repetition frequency is impeded by the aberration loss, which can be reduced by increasing the diameter of the pumped region, which, in turn, will lead to additional energy losses of the pump beam because of its incomplete overlap with the cavity mode in the active medium. In this case, it is necessary to use higher power diode pumping to exceed the lasing threshold.

6. Conclusions

The use of longitudinal pumping by diode bars with a fibre output is promising for designing effective pulse-periodic lasers with a millijoule pulse energy. However, with an increase in the average pump power, the significantly nonuniform radial heating of the laser AE leads to the formation of a large aberration component in the induced thermal lens, as a result of which lasing cannot occur. Stable laser operation can be implemented in a limited repetition frequency range, the boundaries of which are determined by the cavity parameters and the diameter of the pumped region. The conditions of stable lasing at repetition frequencies up to 1 kHz were determined for Nd : YAG and YAG/Nd : YAG laser elements. The character of the manifestation of thermal-lens aberrations for these two elements was experimentally investigated using a

probe beam. The simplest aberration model presented here adequately describes the experimental data and allows one to calculate the optimal cavity configuration for a specified range of pulse repetition frequencies.

Acknowledgements. This study was supported by the Russian Foundation for Basic Research (Grant No. 10-02-01277-a).

References

1. Seeger T., Kiefer J., Leipertz A., Patterson B.D., Kliewer C.J., Settersten T.B. *Opt. Lett.*, **1**, 3755 (2009).
2. Arakcheev V.G., Kireev V.V., Morozov V.B., Olenin A.N., Tunkin V.G., Valeev A.A., Yakovlev D.V. *J. Ram. Spectr.*, **38**, 1046 (2007); **38**, 1052 (2007).
3. Ageeva N.N., Bronevoi I.L., Zabegaev D.N., Krivonosov A.N. *Fiz. Tekh. Poluprovodn.*, **44**, 1328 (2010).
4. Pashchenko V.Z., Grishanova N.P., Noks P.P., Korvatovskii B.N., Rubin A.B. *Elektrokhimiya*, **38**, 103 (2002).
5. Furbach A., Peng X., Turi L., Krausz F. *Appl. Phys. B*, **78**, 261 (2004).
6. Kurtz R.M., Horvath C., Liu H., Krueger R.R., Juhasz T. *J. Refract. Surg.*, **14**, 541 (1998).
7. Targowski P., Ostrowski R., Marczak J., Sylwestrzak M., Kwiatkowska E.A. *Proc. SPIE Int. Soc. Opt. Eng.*, **7391**, 73910G (2009).
8. Kaldvee B., Ehn A., Bood J., Alden M. *Appl. Opt.*, **48**, B65 (2009).
9. Keller U. *Nature*, **424**, 831 (2003).
10. Kovalev V.I., Harrison R.G., Scott A.M. *Opt. Lett.*, **30**, 3386 (2005).
11. Bourderionneta J., Brignona A., Huignarda J.-P., Frey R. *Opt. Commun.*, **204**, 299 (2002).
12. Zverev G.M., Golyaev Yu.D., in *Lazery na alyumooittrievom granate* (Lasers on Aluminum – Yttrium Garnet) (Moscow: Radio i svyaz', 1985).
13. Grechin S.G., Nikolaev P.P. *Kvantovaya Elektron.*, **39**, 1 (2009) [*Quantum Electron.*, **39**, 1 (2009)].
14. Cousins A.K. *Appl. Opt.*, **31**, 7259 (1992).
15. Gorbunkov M.V., Konyashkin A.V., Kostryukov P.V., Morozov V.B., Olenin A.N., Rusov V.A., Telegin L.S., Tunkin V.G., Shabalin Yu.V., Yakovlev D.V. *Kvantovaya Elektron.*, **35**, 2 (2005) [*Quantum Electron.*, **35**, 2 (2005)].
16. Babichev A.P., Babushkina N.A., Bratkovskii A.M. *Fizicheskie velichiny* (Physical Quantities) (Moscow: Energoatomizdat, 1991).
17. Flood C.J., Walker D.R., van Driel H.M. *Opt. Lett.*, **20**, 58 (1995).
18. Mezenov A.V., Soms L.N., Stepanov A.I., in *Termooptika tverdotel'nykh lazerov* (Thermooptics of Solid-State Lasers) (Leningrad: Mashinostroenie, 1986).
19. Weber R., Neuenschwander B., Weber H.P. *Opt. Mater.*, **11**, 245 (1999).
20. Innocenzi M.E., Yura H.T., Fincher C.L., Fields R.A. *Appl. Phys. Lett.*, **56**, 1831 (1990).
21. Kogelnik H., Li T. *Appl. Opt.*, **5**, 1550 (1966).
22. Sanchez F., Brunel M., Ait-Ameur K. *J. Opt. Soc. Am. B*, **15**, 2390 (1998).
23. Akhmanov S.A., Nikitin S.Yu. *Fizicheskaya optika* (Physical Optics) (Moscow: Nauka, 2004).
24. Jabczynski J. *Opt.Commun.*, **182**, 413 (2000).
25. Van den Bos A. *J. Opt. Soc. Am. A*, **17**, 356 (2000).